VOL. 10, NO. 16, SEPTEMBER 2015 ISSN 1819-6608
ARPN Journal of Engineering and Applied Sciences

www.arpnjournals.com

NUMERICAL OPTIMIZATION OF THE SHAPE OF A HOLLOW PROJECTILE

Wessam Mahfouz Elnaggar, Zhihua Chen and Hui Zhang
Key Laboratory of Transient Physics, Nanjing University of Science and Technology, Nanjing, China
E-Mail: Chenzh@njust.edu.cn

ABSTRACT

To reduce the drag of a normal hollow projectile, computational fluid dynamics (CFD) is applied to simulate numerically the flow fields of hollow projectiles with different shapes; the drag coefficients of different projectiles are calculated. The optimal geometry of hollow projectile with the minimum drag coefficient is obtained accordingly. Moreover, with different inflow Mach numbers, the flow fields of both optimal and normal projectiles are simulated and compared, the flow characteristics are discussed, and the drag reduction effect of optimal projectile is validated.

Keywords: hollow projectile, drag coefficient, shock wave, viscosity, flow field.

INTRODUCTION

Hollow projectiles, also known as tubular projectiles, are cylindrical projectiles with a large circular duct along the longitudinal axis [1,2], and their application prospects are very wide in aircraft ammunitions. The hollow projectile has the feature of high precision and small drag coefficient, which attracts much attention.

The circular duct along the longitudinal axis of a hollow projectile which causes low reduction of muzzle velocity and small drag makes its performance greatly improved [3]. Its characteristics, such as a flat trajectory and short flight time caused by high flight velocity, spin stabilization, etc. can ensure not only the high accuracy of hollow projectile but also the low dispersion. Also, hollow projectile has a series of good performance characteristics and operation, such as superior target penetration, inexpensive manufacturing, low recoil, suitable for handling and transportation etc [4].

Many numerical investigations about hollow projectile were performed mainly based on the inviscid Euler equations [5-11]. Actually, the surface of a hollow projectile is about twice of that of normal bullets; therefore, the friction drag caused by the wall surface cannot be ignored. In recent years, the numerical simulations were carried out based on the Navier-Stokes equations, and the main flow structures of the projectile were displayed [6]. However, there are few papers concerning the relationship between the projectile shape and its drag.

In this paper, our purpose is to study the relation between the projectile shape and its drag. A normal hollow projectile is used as the example, through the modification of its geometry, the varied curve of its shape with the drag has been calculated numerically, and the aerodynamic shape with minimum drag has been obtained.

NUMERICAL METHOD

The governing equation used in this paper is the Reynolds Averaged Navier-Stokes equation. The Spalart-Allmaras turbulent model is adopted to close the equations. The convective term is approximated by second order AUSM scheme. The second order central difference scheme is applied to pursue numerical approximation of the viscous term. Runge-Kutta method is applied to step on time.

To validate above method, we use the normal hollow projectile [5] (Figure-1.a) as the example to be simulated numerically at three different mach numbers, the distribution of drag coefficient (Cd) of our numerical results agrees well with that of [5], however, our results are a little larger, the reason is that we use the viscous N-S equations and the inviscid Euler equations is applied in Ref.[5], therefore, the friction drag is ignored in [5].

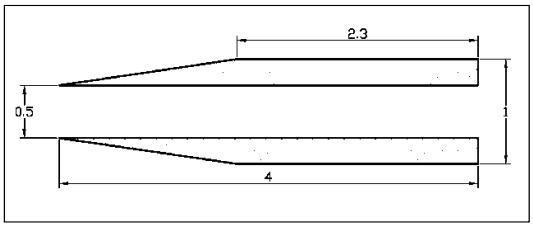

(a) Normal hollow projectile model [5].

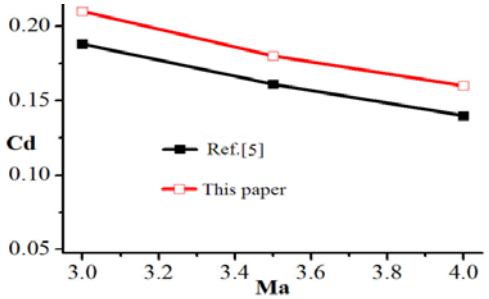

(b) Comparison of drag coefficient at different Mach numbers.

Figure-1. Normal hollow projectile model (a) and drag coefficient at different Mach numbers (b).

For the hollow projectile, three geometric parameters are mostly concerned; they are the external diameter (D), the inner diameter (d) and the length (L). Our numerical simulations show that, the projectile in a cylinder shape has larger drag than that of the cone, therefore, the basic shape of the projectile for our simulation is chosen to be the cone and is shown in Figure-2, where D=30mm，d=17.2mm，L=80mm.

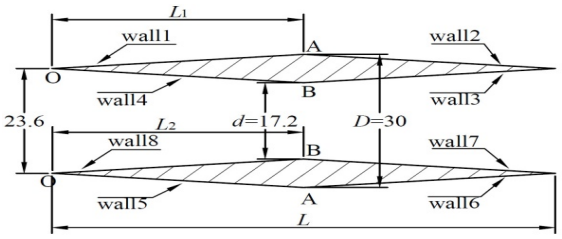

Figure-2. Basic model geometry (all dimensions in millimetres).

RESULTS AND DISCUSSIONS

Numerical Optimization of External Wall

Firstly, we only study the relationship between the geometry of external wall and the projectile drag, and other parameters are chosen to be constant, therefore, we can obtain the variation curve of drag with L_1, and due to the symmetrical shape of the projectile, only the upper half of the projectile is chosen to be discussed. The inflow Mach number is taken to be 3.

Figure-3 illustrates the pressure contours of the projectile with L_1=30, 48 and 70mm. It is clear that with the increase of L_1, the pressure on the external wall of projectile head decreases, however, the inner flow fields do not change, thus, we can consider that the drag changes with the variation of L_1.

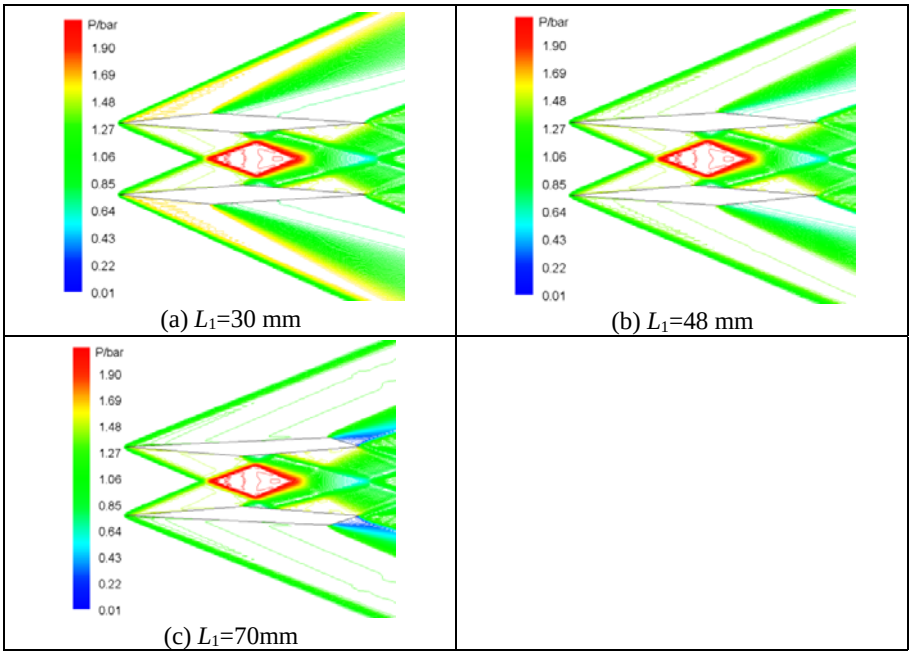

Figure-3. Distributions of the pressure contours with L_1=30, 48 and 70mm.

The pressure drag, friction drag and total drag of external wall with different L_1 are shown in Table 1. The variation of L_1 has little effect on the friction drag and can be neglected, which means the modification of total drag is dominated by the pressure drag.

From Table-1, we also know that the modification of total drag with L_1 is not simple linear, there is a minimum value. To obtain this point, we can decrease the interval of L_1 around this area, like L_1=10, 20, 30, 40, 42, 44, 46, 48, 49, 50, 51, 52, 54, 56, 58, 60 and 70mm, and corresponding values of total drag coefficient (Cd) obtained from our numerical results are shown in Figure-4. It is clear that the drag takes its minimum value at about L_1=48mm. Therefore, the geometric shape design of the external wall should be L_1=48mm.

Table-1. Variations of aerodynamic forces with different L_1.

L_1 (mm)	**Pressure drag** (N)	**Friction drag** (N)	**Total drag** (N)
10	24.193	3.350	27.543
30	8.288	3.758	12.046
48	6.996	3.767	10.763
70	8.965	3.802	12.767

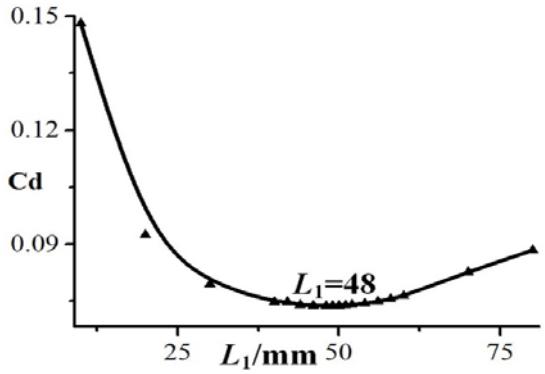

Figure-4. Drag coefficient vs L_1.

Numerical Optimization of Inner Wall

The geometric design of the inner wall can also be obtained based on above process. Firstly, we numerically simulate the flow fields of projectile with L_2=38, 45 and 70mm, and the corresponding pressure contours are shown in Figure-5. It is clear that the external flow field is stable and has nothing to do with L_2. However, the inner flow varies much with different value of L_2. The oblique shock waves of the head collide and interact with each other at the axis and they also interact with the expansion waves which make the inner flow fields much more complicated than external flow.

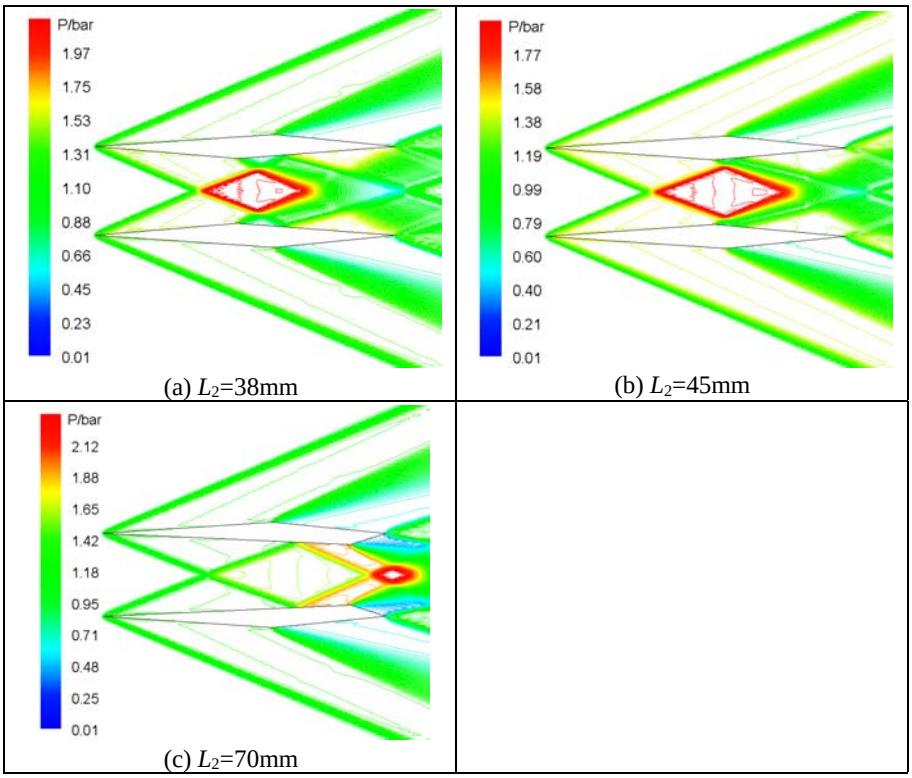

Figure-5. Distributions of the isobars at L_2=38, 45 and 70mm.

The variations of aerodynamic forces with different L_2 can be found in Table-2, and there is also a minimum value of drag for L_2 taking its value around 38mm. Therefore, we can take L_2=10, 20, 30, 35, 36, 37, 38, 39, 40, 41, 42, 43, 44, 45, 50, 60, 70 and 80mm for numerical simulation and their corresponding curve of the total drag coefficient vs L_2=10 is shown in Figure-6. It is also very clear that the drag takes its minimum value at about L_2=38mm. Therefore, the geometric shape design of the inner wall should be L_2=38mm.

Table-2. Variations of aerodynamic forces with different L_2.

L_2 (mm)	**Pressure drag** (N)	**Friction drag** (N)	**Total drag** (N)
20	5.579	4.232	9.811
38	1.616	4.208	5.824
45	1.838	4.145	5.983
70	8.637	4.023	12.660

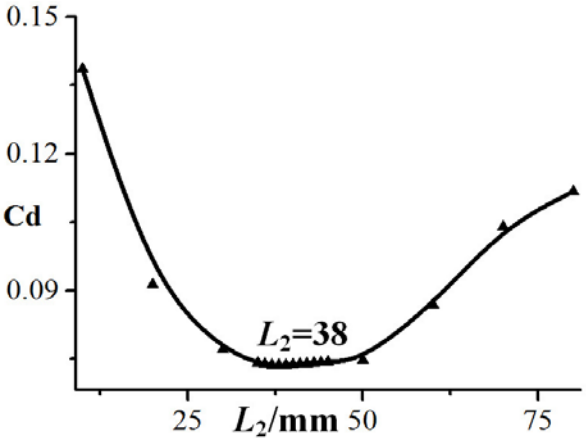

Figure-6. Drag coefficient vs L_2.

The main Characteristics of the Optimal Projectile

Based on above numerical results and discussions, we know the optimal shape of the projectile is L_1=48mm and L_2=38mm, and its configuration is shown in Figure-7. To validate its flight characteristics, the comparison of its flow fields with normal hollow projectile with Ma= 2.5, 3.0 and 4.0 is shown in Figure-7.

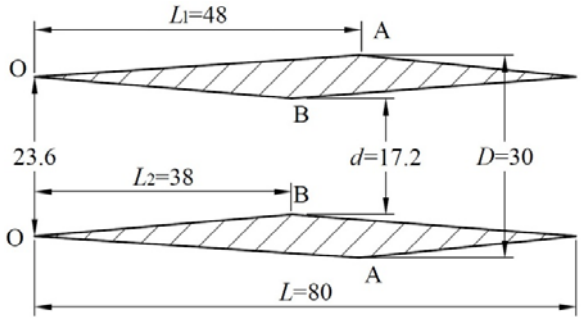

Figure-7. Numerical optimal configuration of the hollow projectile.

From Figure-8, we know the pressure field of the optimal projectile is simpler, especially for its inner flow fields. However, for normal projectile, both the oblique shock waves and expansion waves interact with the others and reflect from the inner walls, which make the flow complex. Moreover, the pressure behind the optimal projectile is high (Figure-8.a), which results in the decrease of pressure drag. However, for normal projectile, the minimum pressure appears at the end of the projectile (Figure-8.b), therefore, its pressure drag is large.

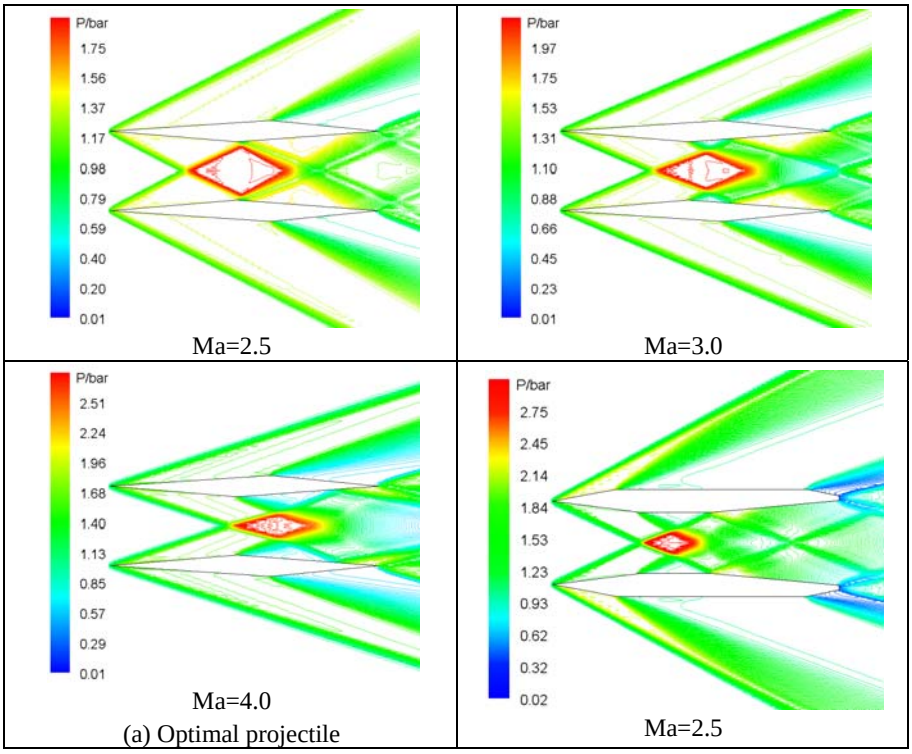

(a) Optimal projectile

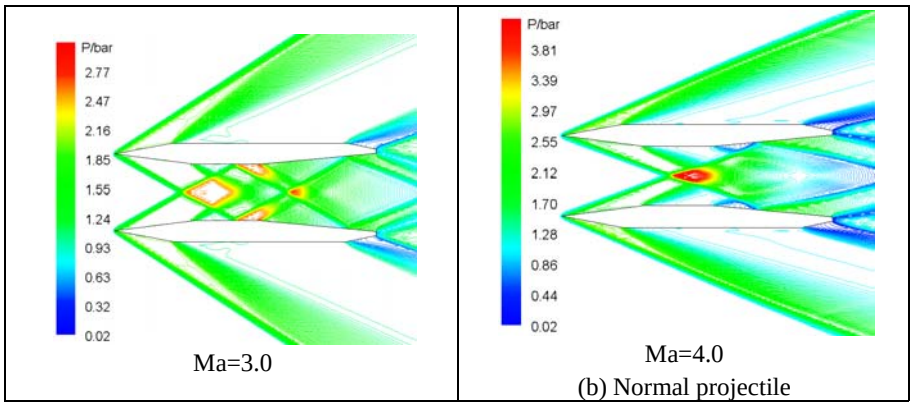

Figure-8. Comparison of pressure field of both the optimal and normal projectiles at Ma=2.5, 3.0 and4.0.

Table-3 displays the Comparison of drags of each portion of both normal and optimal projectiles at Ma=3.0. It shows that the pressure and friction drags of each portion (including the external wall, inner wall and tail) of optimal drag are not larger than that of normal projectile, and the reduced total drag mainly comes from the decrease of pressure drag, the pressure drag of optimal projectile is much less than that of normal projectile, while there is not much difference between their friction drag.

Table-3. Comparison of drags of both normal and optimal projectiles at Ma=3.0.

Portion	External wall		Inner wall		Projectile		
Drag	Pressure	Friction	Pressure	Friction	Pressure	Friction	Total drag
Normal projectile	14.536	3.897	1.814	4.340	18.909	8.237	27.146
Optimal Projectile	6.994	3.767	1.616	4.208	8.610	7.97	16.585

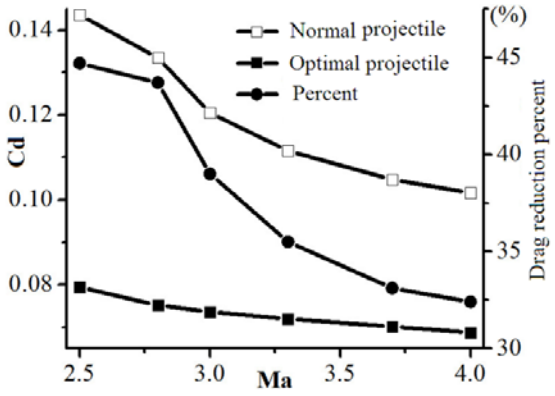

Figure-9. Comparison of drags of both projectile and the drag reduction percent.

To examine further the feature of the optimal projectile, we perform the numerical simulations of both optimal and normal projectile at Ma=2.5, 2.8, 3.0, 3.3, 3.7 and 4.0, and the comparison of drags of both projectiles and the drag reduction percent are shown in Figure-9. It is clear that the drag is obviously low for the optimal projectile even for different Mach numbers, and the drag reduction percent is larger than 30%.

Figure-10 shows the variation of drag and lift coefficients with changing angles of attack at different Mach numbers. As shown in Figure-10.a, the change of the drag coefficient shows the same trend of parabolic curve with different angles of attack for different Mach numbers. The drag coefficient curve is characterized by a slightly sharp rise with increasing angle of attack at the same Mach number. The dominant reason is that for none zero angle of attack, the flow field asymmetry on the projectile walls increasing the pressure drag. As the angle of attack increases, both of the acceleration of pressure drag and the flow field asymmetry increases. In addition, the variation in drag coefficient is relatively small at the same angle of attack, but slightly increases as the Mach number increases. Figure-10.b shows the lift coefficients increase in a linear manner at the same angle of attack for various values of the Mach numbers. While, for the same angle of attack the change in lift coefficients with different Mach numbers is relatively small. Thus, the angle of attack is seen to have more important effect on the lift coefficient than the Mach number.

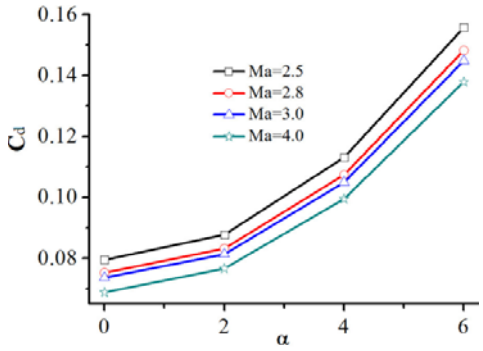

(a) Drag Coefficients

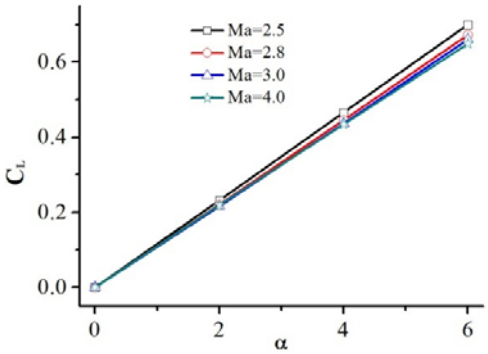

(b) Lift Coefficients

Figure-10. Drag and lift coefficients vs angle of attack at different mach numbers.

Even the hollow projectile fly usually at Mach number among 2.5-4.0, its flight features at lower Mach number are still worth studying. Pressure contours at Mach numbers of 1.2, 1.5 and 1.7 are illustrated in Figure-11. As it is shown, a bow shock appears in front of the projectile at lower Mach numbers, however, and its angle decreases with the increase of the Mach numbers. In addition, with the increase of Mach numbers (Fig.2.a-c), the distances between the bow shock wave and the projectile decrease, and the bow shock wave will turn into the oblique shock wave for large Ma numbers.

On the other hand, The highest pressure location will change with the increase of the Mach number, if there is a bow shock wave, the highest point is at the apex of the projectile, however, with the disappearance of the bow shock (Figure-2), the highest place will move into the hollow projectile (Figure-8), and the values of the highest pressure of the flow fields increases when the bow shock moves close to the projectile (Figures 2.a-c), and it suddenly decreases when it moves into the hollow projectile (Figure-8).

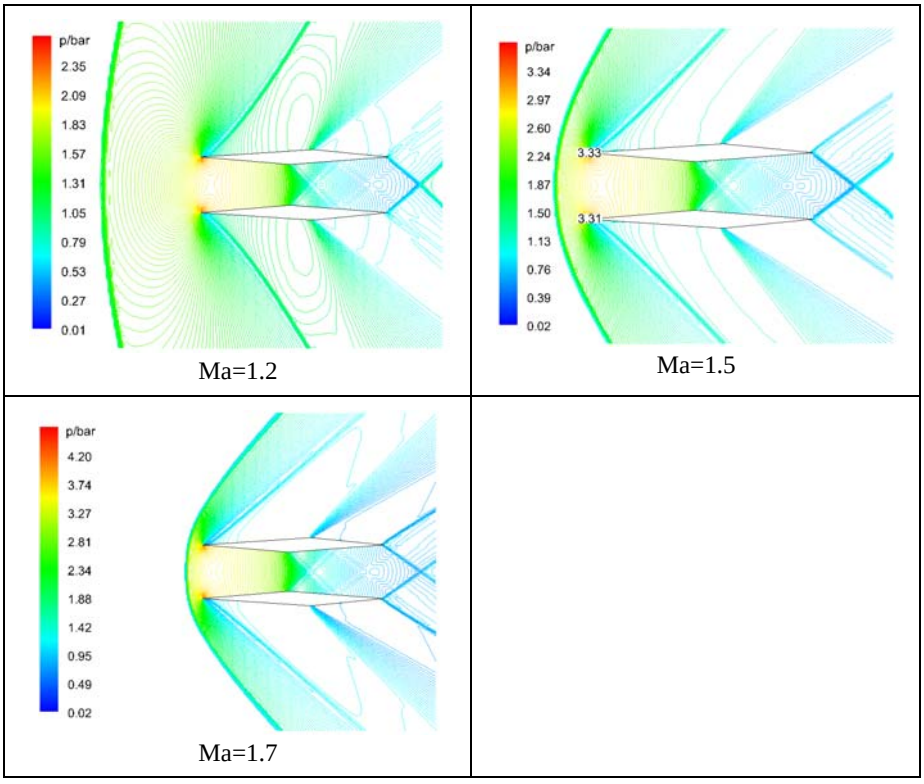

Figure-11. Pressure contours at mach numbers of 1.2, 1.5 and 1.7.

There total drag coefficient consists of two components: pressure drag coefficient and friction drag coefficient. For two different Mach number, Ma=1.5 and 3.0, the change of pressure and friction drag coefficients on the half top of the hollow projectile is shown in Table 1. The pressure drag coefficient on outer walls of hollow projectile at Ma=3.0 is larger than the one at Ma=1.5. However, the force on inner wall3 is in opposite direction of the force on the other walls, which actually becomes the thrust force (pressure drag coefficient is negative). On wall4 the pressure drag coefficient at Ma=3.0is much less than the one at Ma=1.5. As a result, the pressure drag coefficient at Ma=3.0 is much less than at Ma=1.5.

On the contrary, the friction drag coefficient is different from pressure drag coefficient on the outer and inner walls, the friction drag coefficient at Ma=3.0 is larger than the one at Ma=1.5. But the total drag coefficient at Ma=3.0 is smaller than the one at Ma=1.5; because the velocity gradient on boundary layer differs greatly at different Mach numbers. Although the friction drag coefficient is a little high at Ma=3.0 than the one at Ma=1.5, but the total drag coefficient at Ma=1.5 is much larger than at Ma=3.0. That is to say that the percentage of pressure drag coefficient in total drag coefficient is much larger than friction drag coefficient.

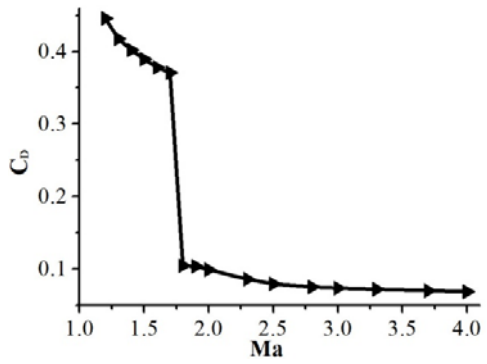

Figure-12. Total drag coefficients versus mach numbers.

Figure-12 shows the total drag coefficients varying with Mach numbers. As we can see, for supersonic flows, the total drag coefficients of hollow projectiles decrease as Mach number increases. And there is a large decrease of drag with the disappearance of the bow shock wave. Generally, the total drag coefficients in detached shock wave (low Mach number) are much larger than the oblique shock wave cases (high Mach number). Therefore, the ideal flight conditions of a hollow projectile are at high Mach numbers.

CONCLUSIONS

The flow fields of hollow projectile at supersonic conditions are investigated numerically with the use of Navier-Stokes equation, Spalart-Allmaras turbulent model, and AUSM scheme. The optimal geometric hollow projectile with the smallest drag has been obtained through numerical simulations. To validate the flow features of the optimal hollow projectile, the comparisons of drag between the normal and optimal projectile have been illustrated and the drag reduction effects at different Mach numbers have been obtained, it is larger than 30%. On the other hand, the flow structures of optimal projectile at low Mach numbers have been simulated numerically. The bow shock wave structure and its variation with Mach number have been discussed. Finally, we obtained the variation of projectile drag versus Mach number.

ACKNOWLEDGEMENT

This work was supported by the National Natural Science Foundation of China under Grant No. 11272156.

REFERENCES

[1] L. M. Sadowski, E. T. Malatesta, J. Huerta. 1984. 30-mm Tubular Projectile, US Patent, ADB087370.

[2] H. Li, J. Yang, R. Qi. 1980. Hollow Projectile Study, Acta Armamentarii. 2: 33-41(in Chinese).

[3] C. Berner, M. Giraud. 1989. Supersonic Wind Tunnel Investigation of a Tubular Projectile. Proceedings of the 11th International Symposium on Ballistics, Brussels, Belgium.

[4] Y. Wang. 1996. Studying Progress on Hollow Projectile Technique in the Western Countries. Projectile and Rocket Technology. 9(3): 1-10.

[5] J. Evans. Prediction of Tubular Projectile Aerodynamics Using the ZUES Euler Code. AIAA 89-0334. Reno, Nevada.

[6] F. Lesage. M.J. Raw. Computational Fluid Dynamic Applications of a Navier-Stokes Code in External Ballistics. AIAA 92-0637. Reno, Nevada.

[7] Y. Li, Z. Chen. 2011. Aerodynamic Characteristics of Hollow Projectile with a Diameter of 30 mm under Real Conditions. Aeronautical Computing Technique. 41(5): 76-80. (in Chinese).

[8] D. Ren, J. Tan, J. Zhang. 2006. Flow Filed Simulation Hollow Projectile Using Implicit Method Base on Unstructured Meshes. Mechanics in Engineering. 28(5): 24-27. (in Chinese).

[9] X. Gao, J. Qian, X. Wang. 2005. Flow field Calculation and Drag Characteristic of Hollow Projectile, Journal of Nanjing University of Science and Technology. 29(2): 158-161. (in Chinese).

[10] J. Qian, Y. Li, Z. Chen, The Investigation on Flow Characteristics of a Low-drag Hollow Projectile. Journal of Projectiles, Rockets, Missiles and Guidance. 31(4): 73-75. (in Chinese).

[11] Z. Huang, Y. Li, Z. Chen. 2013. Numerical Optimization of the Aerodynamic Configuration Design of a Hollow Projectile Based on its Drag Coefficient, Acta Armamentarii. 34(5): 535-540. (in Chinese).